Bulk FePt-based nanocomposite magnets with enhanced exchange coupling

Chuan-Bing Rong, Vikas Nandwana, Narayan Poudyal, and J. Ping Liu[a)]
Department of Physics, University of Texas at Arlington, Arlington, Texas 76019

Mikhail E. Kozlov and Ray H. Baughman
NanoTech Institute, University of Texas at Dallas, Richardson, Texas 75083

Yong Ding and Zhong Lin Wang
School of Materials Science and Engineering, Georgia Institute of Technology, Atlanta, Georgia 30332

High density bulk $FePt/Fe_3Pt$ nanocomposite magnets have been prepared by high-pressure warm compaction of chemically synthesized FePt and Fe_3O_4 nanoparticles. It is found that the density increases with the compaction pressure and temperature. Density of the bulk samples up to 95% theoretical value has been obtained while the nanostructured morphology is retained. It is also observed that a high pressure expedites the FePt phase transition from the disordered face-centered-cubic structure to the $L1_0$ structure, leading to the phase transition temperature in the compacts one hundred degrees lower than usual. This phase transition in turn facilitates the consolidation of the compacts. Magnetic characterizations showed that interphase exchange coupling is enhanced upon the compaction. Post-annealing of the compacts results in further improved magnetic performance of the compacts owing to interface modification. Energy products up to 16.3 MG Oe of the isotropic bulk nanocomposite magnets have been achieved, which is significantly higher than the theoretical limit for fully dense single-phase FePt magnets. © *2007 American Institute of Physics.*
[DOI: 10.1063/1.2756619]

I. INTRODUCTION

Exchange-coupled hard/soft nanocomposite magnets have attracted great interest[1–4] in the last decade because of their potential in achieving giant energy product $(BH)_{max}$ that may be as large as 100 MG Oe.[5,6] Effective interphase magnetic exchange coupling in the nanocomposites can be achieved if dimensions of the soft-phase components are not larger than a nanoscale critical length.[7–12] The grain size in nanocomposite magnets fabricated by conventional top-down methods, including mechanical alloying and rapid quenching, usually has a wide distribution, and can hardly be controlled below the critical length. An alternative bottom-up approach therefore is necessary to fabricate nanocomposite magnets with controllable nanoscale morphology. Recently, magnetic FePt nanoparticles synthesized by chemical solution methods have aroused significant attention because of their very small particle size and size distribution, which make them ideal building blocks for exchange-coupled nanocomposite bulk magnets.[13–16] The biggest challenge for the bottom-up approach is how to produce bulk nanostructured magnets without losing the homogenous nanoscale morphology. Conventional compaction and condensation techniques cannot be applied for nanoparticles since those techniques require extensive heat treatments which lead to excessive grain growth. To date, there have been very limited data reported on direct compaction of intermetallic nanoparticles, especially for nanoparticles with size down to several na-

nometers. Recent attempts to fabricate bulk nanostructured magnets by using unconventional compaction techniques including plasma sintering and dynamic compaction[17,18] have resulted limited success. Bulk samples with density up to 80% theoretical value have been obtained. The challenge remains in producing bulk nanostructured magnets with density close to theoretical values.

On the other hand, the as-synthesized FePt nanoparticles have the disordered face-centered cubic (fcc) structure with vanishing magnetocrystalline anisotropy. High temperature annealing (above 600 °C) is necessary to obtain the ordered $L1_0$ structure with very high magnetocrystalline anisotropy for hard magnetic applications. The challenge is how to avoid excessive particle or grain growth at such high temperatures. Adding third elements is one possibility to reduce the ordering temperature, while it inevitably decreases the magnetization which is harmful for applications as permanent magnets.[23,24] Since the high pressure may reduce the phase transition temperature,[25] the high-pressure warm compaction is therefore considered to be applicable to fabrication of nanoparticle based composite magnets.

High-pressure warm compaction is one of the advanced compaction techniques in powder metallurgy and has been widely used in automobile parts manufacturing in the past decade.[19–22] This technique is established on the knowledge that metallic powders have better plasticity and compressibility at elevated temperatures and therefore are easier to be deformed to form high density bulks under a certain pressure, compared with cold pressing. Unlike hot pressing,

---

a)Electronic mail: pliu@uta.edu

102, 023908-1

warm compaction is performed at modest temperatures at which the metallic powders are chemically stable and no excessive grain growth occurs.

In this work, we report our recent results in preparation and characterization of bulk FePt/Fe$_3$Pt nanocomposite magnets by compacting chemically synthesized FePt and Fe$_3$O$_4$ nanoparticles at modest temperatures.

II. EXPERIMENTAL

The nanoparticles were synthesized by standard airless chemical solution procedures.[13,26,27] The FePt with fcc structure and Fe$_3$O$_4$ nanoparticles were mixed at a mass ratio of 8:1 in a solution before centrifugation. The dried nanoparticles were heated under Ar atmosphere at 350 °C for 1 h to remove surfactants. The powders were then compacted with a warm-compaction press under pressure of 2.5 or 3.8 GPa for 10 min at temperatures ranging from room temperature (about 20 °C) to 600 °C. The obtained bulk samples had dimensions ϕ6 mm$\times$1.5 mm and ϕ3 mm$\times$1.2 mm for the compaction pressures of 2.5 and 3.8 GPa, respectively. For comparison, we also compacted 15 nm $L1_0$ FePt nanoparticles prepared by the salt-matrix annealing technique[16,28] at 2.5 GPa pressure. The Archimedes method was employed for measurements of bulk sample density. The morphology and crystalline structure were characterized by scanning electron microscopy (SEM), transmission electron microscopy (TEM), and x-ray diffraction (XRD) using Cu K_α radiation. The composition of the compacted samples were checked by energy dispersive x-ray (EDX) analysis in SEM. Magnetic properties were measured with superconducting quantum interference device magnetometer with a maximum applied field of 70 kOe.

III. RESULTS AND DISCUSSIONS

A. Density

It is known that the limit for density ρ_p of a randomly packed particle system is only 64% if no deformation is involved.[29] To obtain a higher ρ_p, it is necessary to realize plastic deformation of the particles. For nanoparticles, the deformation will not be as easy as for large particles because of the reduced dislocations in the particles, which explains low density values obtained in nanoparticle compacts. Figure 1 shows the dependence of ρ_p of the bulk samples on the compaction temperature (T_{cp}) under different pressures. One can see that the density increased monotonously with compaction temperature for both fcc and $L1_0$ particle compacts. The samples prepared at pressure 3.8 GPa and T_{cp} of 600 °C has the highest density (13.8 g/cm^3) which is about 95% of the full density value (14.5 g/cm^3 for the FePt/Fe$_3$Pt composite with 15% volume fraction of Fe$_3$Pt phase). Such high density is a result of a significant plastic deformation of the nanoparticles at the applied high pressure. A linear increase in the density can be observed for the $L1_0$ particles in the whole studied temperature range and for the fcc particles in the temperature range from 20 to about 400 °C. This may be explained by the fact that the yield strength of metallic FePt materials decreases linearly with temperature in the region between 20 and 800 °C (Ref. 30) and an effective lubrica-
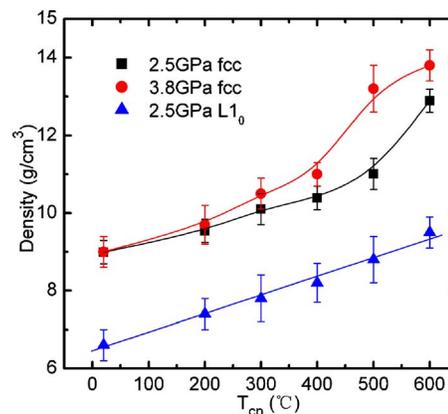
FIG. 1. (Color online) The dependence of density of the bulk samples on compaction temperature T_{cp}.

tion mechanism can occur in the heated powders.[19] However, this linear increase in density did not lead to full densification, even one extrapolate the curve to a high temperature.

Figure 1 shows that for the fcc nanoparticles, the dependence of ρ_p on T_{cp} became steeper when $T_{cp} \geq 400$ °C. This nonlinear behavior may be related to the phase transition from the disordered fcc to the ordered $L1_0$ structure during which atoms are activated and become more mobile. The enhanced atomic diffusion promoted densification of the compacts and resulted in high density. On the other hand, the phase transition may also accelerate the formation of Fe$_3$Pt phase in the FePt-Fe$_3$O$_4$ nanoparticle system.[14] Approximately 15% volume fraction of Fe$_3$Pt phase was determined by using the method of Rietveld refinement of the XRD pattern which will be discussed later.

SEM analysis was performed on the fracture surfaces of the compacts to characterize morphological changes in the compacted samples. Figure 2 shows the typical SEM images of the bulk samples compacted at 20, 400, and 600 °C. The 20 °C-compacted samples are quite porous. With increasing T_{cp} to 400 °C, it is interesting to find that stripes with thickness around 10–20 μm were formed. However, some small holes were still found in the layers. Compacting at 600 °C led to very large and homogenous areas ($>$150 μm) in the compact and thus the high density. The SEM morphology change agrees with the dependence of density on compacted temperature as shown in Fig. 1.

B. Phase transition

As mentioned earlier, the rapidly increased density at the compaction temperature higher than 400 °C may be related to the phase transition of FePt component from fcc structure
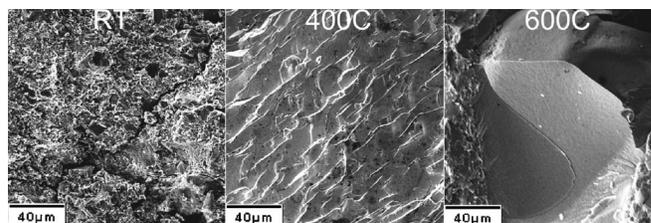
FIG. 2. SEM images of the bulk samples compacted at 20, 400, and 600 °C.
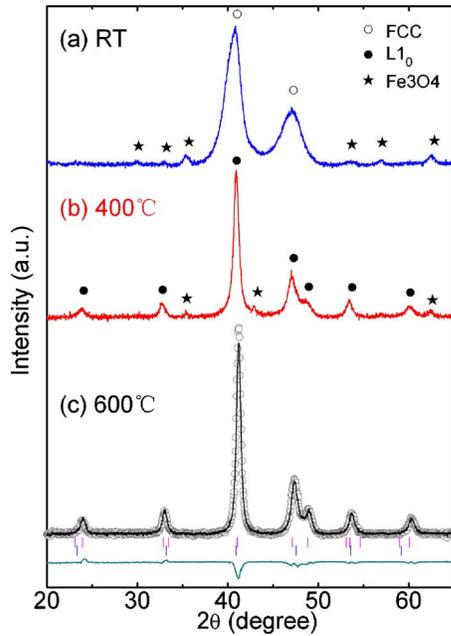
FIG. 3. (Color online) XRD patterns of the bulk samples compacted at (a) 20, (b) 400, and (c) 600 °C. The Rietveld refinement data are also included in (c) for the 600 °C-compacted sample. The symbol (○) and full line represent the observed and calculated x-ray diffraction profiles, respectively. The vertical bars represent the Bragg reflection positions of the observed phases (from top to bottom: $L1_0$ FePt and Fe_3Pt). The difference curve is plotted in the bottom.

to the $L1_0$ structure. To study the phase transition, we performed XRD measurement of the 20, 400, and 600 °C-compacted samples and the patterns are shown in Fig. 3. It can be seen that the 20 °C-compact mainly consists of fcc FePt and Fe_3O_4 phases. The compaction at 400 °C led to the phase transition of FePt component from fcc to $L1_0$ structure while Fe_3O_4 was still existing. With increasing T_{cp} to 600 °C, the FePt phase is of $L1_0$ structure and the Fe_3O_4 disappeared. The quantitative analysis of the phase content can be made approximately by using the method of the Rietveld refinement on XRD patterns.[31,32] As an example, the Rietveld refinement data of the 600 °C compact is also shown in Fig. 3. The SEM/EDX analysis shows the decrease of oxygen content from 13.7% for the 20 °C-compacted sample to 5.0% for the 600 °C-compacted sample based on big regions. Especially, the oxygen content decreases fast when $T_{cp} \geq 400$ °C, which implies that the nanocrystalline Fe_3O_4 decomposed during the compaction at a temperature much lower than that reported in the literature.[33] The TEM/ EDX analysis based on small regions confirms the existence Fe_3Pt grains in the 600 °C-compacted samples. The real cause for the decomposition of Fe_3O_4 remains to be understood and it may be related to the activated atoms diffusion during the phase transition of FePt component.

To evaluate the degree of phase transition from the disordered fcc to the ordered $L1_0$ structure in a quantitative way, the chemical ordering parameter S has been calculated by $S \cong 0.85[I_{001}/I_{002}]^{1/2}$ for the compacts and starting powders, where I_{001} and I_{002} are the integrated intensity of (001) and (002) XRD peaks of the $L1_0$-FePt phase, respectively.[34–36] Figure 4 gives the dependence of S on the compaction tem-
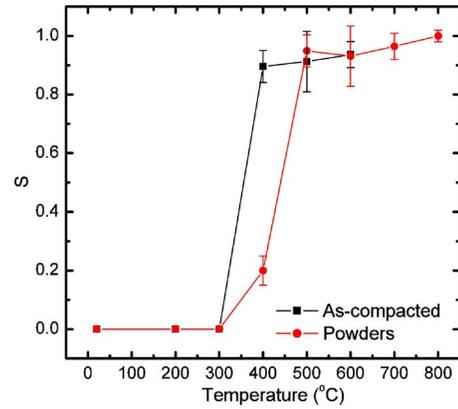
FIG. 4. (Color online) The dependence of S on T_{cp} for the bulks. For comparison, the dependence of S on annealing temperature of the starting powder is also included for 10 min annealing.

perature. It shows clearly that S was almost zero when $T_{cp} \leq 300$ °C while it jumped to 0.9 at $T_{cp} = 400$ °C, indicating that the phase transition from fcc to $L1_0$ was almost completed for the 400 °C-compacted samples. For comparison, the dependence of S on the annealing temperature of the starting powders is also given in Fig. 4, where the annealing time is 10 min, which is same as the compacting time. It is interesting to note that the phase transition took place at a temperature (≤ 400 °C) in the compacts lower than the powders and that reported for the FePt thin films (usually around 600 °C).[37] The presence of pressure should be responsible for the phase transition temperature shift. The expedited phase transition under high pressure is likely associated with the fact that the phase transition can be described as a compression of the fcc structure in the direction of the c axis of the resulted tetragonal phase.

The phase transition is also confirmed by the dependence of magnetic properties on T_{cp}. Figure 5 shows the dependence of saturation magnetization M_s (measured in an applied field of 7 T) and coercivity H_c on T_{cp}. The samples compacted at relatively low temperatures ($T_{cp} < 400$ °C) showed nearly zero coercivity, while the 400 °C-compacted sample gave H_c of 10 kOe. The drastic increase in coercivity originated from the formation of the $L1_0$ phase with high magnetocrystalline anisotropy. Since a higher T_{cp} led to a higher density of the compacts and thus a reduced surface effect,[16,38] the M_s value was increased from 850 to
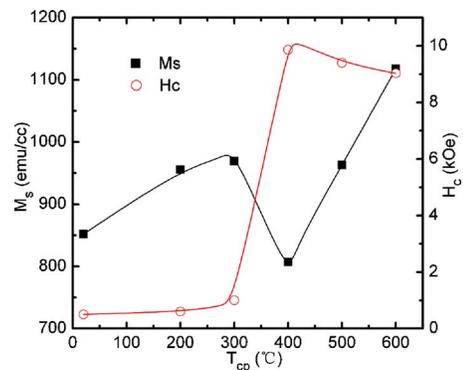
FIG. 5. (Color online) The dependence of M_s and H_c on T_{cp}.
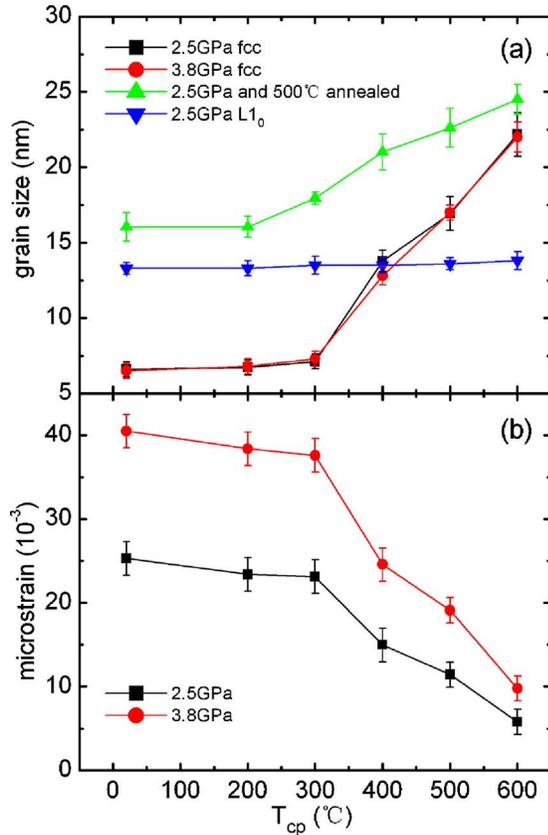
FIG. 6. (Color online) The dependence of grain size and microstrain on T_{cp} for as-compacted samples. The grain size of the annealed samples and the compacted $L1_0$ nanoparticles are also given.

FIG. 7. TEM micrographs of bulk samples compacted at different temperatures. (a) 20, (b) 400, (c) 600 °C, and (d) SAED patterns at different temperatures.

970 emu/cm^3 with increasing T_{cp} from 20 to 300 °C. However, the M_s dropped to 800 emu/cm^3 at T_{cp}=400 °C, which can be attributed to the phase transition since the antiparallel alignment of the polarized Pt spins to the Fe spins in the $L1_0$ ordered FePt alloys and thus M_s of the $L1_0$ phase is lower than that of the fcc phase.[39–41] Similar results were reported in Ref. [41], where the M_s decreased by about 30% from 1000 emu/cm^3 of the fcc phase to 670 emu/cm^3 of the $L1_0$ phase. Considering the FePt/Fe$_3$O$_4$ mass ratio of 8:1 in our samples, the decrease of M_s should be 23% if the fcc phase is completely transferred to the $L1_0$ phase, which is in good agreement with the observed result. The further increase of T_{cp} resulted in a fast increase of M_s, due to the decomposition of magnetite and the formation of Fe$_3$Pt phase during the compaction at relatively high temperature.

C. Microstructural characteristics

To quantitatively determine the effect of warm compaction on the microstructure, x-ray diffraction line-broadening analysis was performed on the bulks. The grain size and retained strain were then determined using the Williamson–Hall analysis method.[42] Figure 6 shows the dependence of grain size and microstrain on the compaction temperature for both 2.5 and 3.8 GPa-compacted samples. As one can see from Fig. 6(a), the grain size was almost unchanged (around 7 nm) with temperature when $T_{cp}\leq$300 °C. However, the grain size increased linearly after that to 22 nm when T_{cp}=600 °C. It is interesting to note that the pressure has little

effect on the grain size. On the other hand, it is obvious that the phase transition promoted grain growth which can be seen from the abrupt increase in grain size after the temperature was higher than 400 °C. Nevertheless, the grain size is still under control in the nanoscale. It is also noted that a higher pressure led to a higher microstrain in the compacts and the microstrain was reduced with increasing temperature. When the temperature was increased to $T_{cp}\geq$400 °C, the microstrain was reduced quickly, as shown in Fig. 6(b), since the atomic rearrangement and atomic diffusion during the phase transition released the strain in the samples.

The grain size of bulk samples with post-annealing (compacted under 2.5 GPa and annealed in forming gas at 500 °C for 1 h) was also included in Fig. 6 to illustrate the effect of heat treatment on the morphology. It is found that the annealing led to the grain growth from 6.5 to 16 nm for the 20 °C-compacted sample, while only from 22 to 25 nm for the 600 °C-compacted sample, implying that the phase transition is the main reason for the grain growth. This is also evidenced by the observation that grain size of the $L1_0$ nanoparticles was almost unchanged during the annealing. The compacts made by the 15 nm $L1_0$ nanoparticles showed no grain growth up to 600 °C (see Fig. 6). To confirm this observation, we heated the samples to 1000 °C for 1 h and found that the average grain size was just slightly increased to about 17 nm. The high stability of the $L1_0$ structured nanoparticles can be utilized for fabrication of bulk nanocomposite magnets with very fine and homogenous nanoscale morphology.

Figure 7 shows the bright field TEM images of the bulk samples prepared from fcc nanoparticles under 2.5 GPa pressure at 20, 400, and 600 °C. The selected area electron diffraction patterns [Fig. 7(d)] confirm the phase transition. The TEM images show that grain size increases with T_{cp} as ex-

pected. The grain size is about 7 ± 3 nm and 14 ± 5 nm for the 20 and 400 °C-compacted samples, respectively. The grain size and size distribution are quite small compared to those for bulk materials fabricated by traditional techniques. This is in agreement with Fig. 6 that exhibits the dependence of average grain size on the compacting temperature. For the 600 °C-compacted samples, TEM image shows the grain size is about 30 ± 10 nm, which is larger than that of XRD analysis. This should be attributed to the existence of large number of twin grains as marked in the Fig. 7(c).

D. Exchange coupling and magnetic properties

All the efforts in controlling grain size are made for the purpose to realize intergrain magnetic exchange coupling and thus to achieve high energy products. To study the magnetic interactions in the warm compaction-produced nanocomposite magnets, the $\delta m = m_d(H) - [1 - 2m_r(H)]$ measurements (Henkel plots) were performed.[43–45] Here m_d is demagnetization remanence and m_r is isothermal magnetization remanence. Both of these values are normalized by the saturation remanence. Nonzero δm is caused by magnetic interactions between particles or grains. The positive δm is interpreted as a sign for magnetic exchange coupling and the negative δm is a sign of magnetic dipolar interaction. Figure 8(a) shows δm plots of 400 and 600 °C-compacted samples prepared from the fcc particles. The δm value for the 600 °C-compacted sample is positive and much higher than that for the 400 °C-compacted sample, indicating stronger exchange coupling in the compact compared to the 400 °C-compacted samples with lower density. This is also reflected by the shape of the hysteresis loops, as shown in the inset of Fig. 8(a). The remanence ratio (M_r/M_s=0.63, where M_r is the remanent magnetization) of the 600 °C-compacted sample is higher than that of the 400 °C compacted (0.58), which is also consistent with the δm measurement. This effect is even more pronounced for the $L1_0$ particle samples. Figure 8(b) shows the Henkel plots for 15 nm $L1_0$ nanoparticles and their compacts. δm for them before compaction is a large negative value. After the compaction at 2.5 GPa and 200 °C, δm changed its sign to positive, indicating an interparticle exchange interaction. Annealing of the compact at 1000 °C for 1 h led to further increase in δm value and thus an enhancement of the exchange coupling. As the annealing causes almost no obvious grain growth, the strong increase in δm can be attributed to improvement in interface conditions upon the high temperature annealing. This result is consistent with the results reported in Ref. 46. The inset in Fig. 8(b) gives the hysteresis loops of the $L1_0$ nanoparticles and its compacts. It shows that the enhanced exchange coupling significantly improves the squareness of the hysteresis loops and therefore the energy products. A $(BH)_{max}$ about 15.6 MG Oe has been obtained based on the measurement from the real density.

The magnetic properties can be further improved by a post-annealing under forming gas (93%Ar+7%H_2) for 1 h. Figure 9 shows the effect of annealing temperature (T_a) on M_s, H_c, and $(BH)_{max}$ of the 20, 400, and 600 °C compacts. As shown in Fig. 9(a), M_s of the 20 and 400 °C compacts
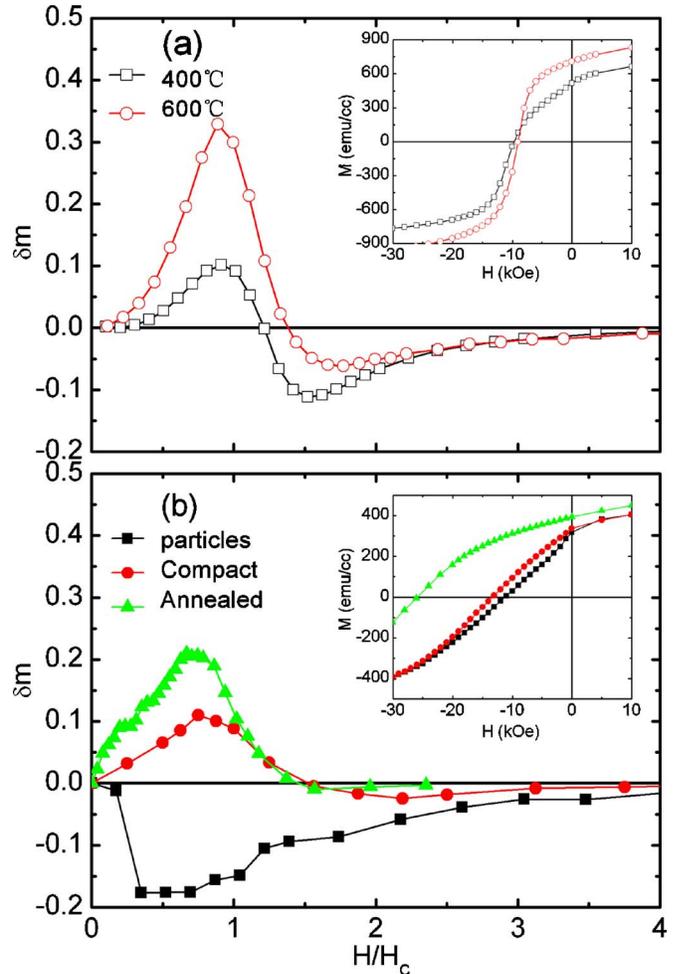
FIG. 8. (Color online) (a) δm plots of the samples compacted at 400 and 600 °C from the fcc nanoparticles. (b) δm plots of the separated $L1_0$ particles and samples compacted (at 2.5 GPa, 200 °C) from the $L1_0$ nanoparticles as well as the post-annealed bulk samples. The insets are the corresponding demagnetization curves.

increased significantly after the annealing. This was attributed to the decomposition of Fe_3O_4 phase and the formation of Fe or Fe_3Pt with high magnetization in the reducing atmosphere. M_s value up to 1140 emu/cm^3 can be obtained by post-annealing. However, it is found that M_s of the 600 °C-compacted sample had a very small change upon post-annealing. This may be due to the early formation of Fe_3Pt phase during the warm compaction as discussed early. For all the samples compacted at the three temperatures, high-temperature annealing (>600 °C) led to a decrease in M_s, which may be related to the atomic diffusion between FePt and Fe_3Pt.[32] As shown in Fig. 9(b), H_c of the 20 °C-compacted samples increases fast when T_a is higher than 450 °C which shows that the phase transition from fcc to $L1_0$ resulted in magnetic hardening. For the 400 and 600 °C-compacted samples, post-annealing did not improve the H_c since the phase transition had already happened during the warm compaction. In this case, high-temperature annealing led to an overgrowth in grain size and therefore deterioration in the magnetic properties. By optimizing the post-annealing parameters further improvement of the $(BH)_{max}$ up to 16.3 MG Oe (based on the real density for
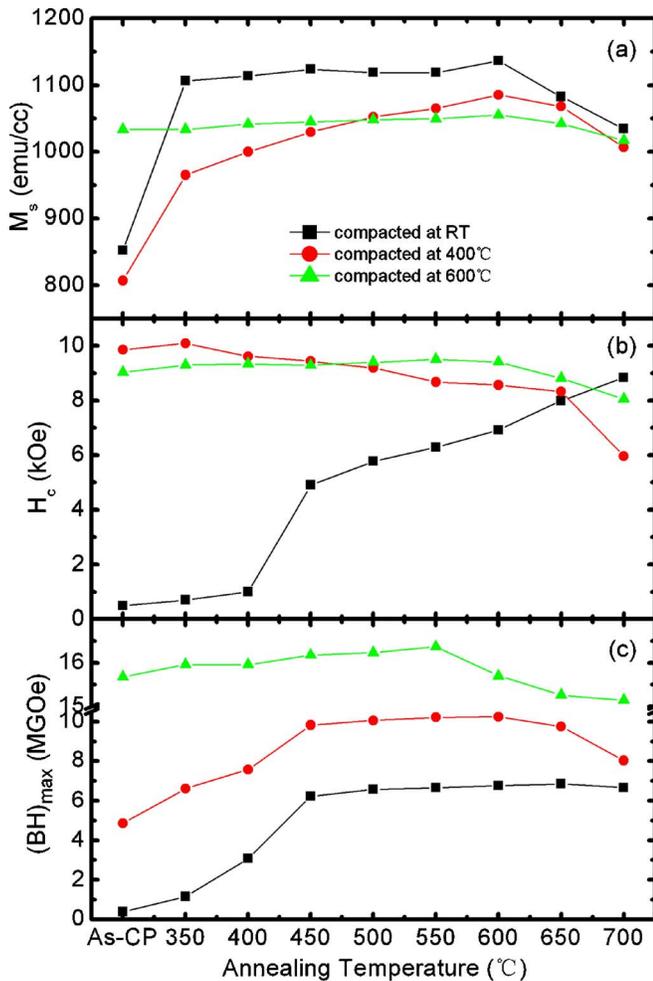
FIG. 9. (Color online) The dependence of M_s, H_c, and $(BH)_{max}$ on the annealing temperature for 20, 400, and 600 °C-compacted samples.

600 °C compact) has been achieved which is significantly higher than the theoretical limit (13 MG Oe) for the single-phase isotropic FePt magnets.

IV. CONCLUSIONS

In summary, high density FePt/Fe$_3$Pt bulk nanocomposite magnets have been obtained by the warm compaction method. A density up to 95% of the full density has been achieved while the nanoscale morphology is retained. Effective exchange coupling in the high-density bulk samples is realized. It is found that the pressure expedites the fcc-$L1_0$ phase transition. The phase transition temperature shifts to a temperature lower than 400 °C under 2.5 GPa pressure. The phase transition has a positive effect on consolidation of the compacts. It has also been observed that the $L1_0$ nanoparticles have high stability during heat treatments. Followed by a proper post-annealing treatment, magnetic properties of bulk samples can be significantly improved. Our results show that warm compaction technique is promising for producing high performance bulk nanocomposite magnets for advanced applications.

[1] R. Coehoorn, D. B. de Mooij, and C. de Waard, J. Magn. Magn. Mater. **80**, 101 (1989).
[2] A. Manaf, R. A. Buckley, and H. A. Davies, J. Magn. Magn. Mater. **128**, 302 (1993).
[3] G. C. Hadjipanayis, J. Magn. Magn. Mater. **200**, 373 (1999).
[4] J. Zhang, S. Y. Zhang, H. W. Zhang, and B. G. Shen, J. Appl. Phys. **89**, 5601 (2001).
[5] R. Skomski and J. M. D. Coey, Phys. Rev. B **48**, 15812 (1993).
[6] C. B. Rong, H. W. Zhang, R. J. Chen, S. L. He, and B. G. Shen, J. Magn. Magn. Mater. **302**, 126 (2006).
[7] E. Kneller and R. Hawig, IEEE Trans. Magn. **27**, 3588 (1991).
[8] Z. J. Guo, J. S. Jiang, J. E. Pearson, S. D. Bader, and J. P. Liu, Appl. Phys. Lett. **81**, 2029 (2002).
[9] Z. S. Shan, J. P. Liu, M. Vamsi Chakka, H. Zeng, and J. S. Jiang, IEEE Trans. Magn. **38**, 2907 (2002).
[10] C. B. Rong, H. W. Zhang, X. B. Du, J. Zhang, S. Y. Zhang, and B. G. Shen, J. Appl. Phys. **96**, 3921 (2004).
[11] R. Skomski, J. Phys.: Condens. Matter **15**, R841 (2003).
[12] A. J. Zambano, H. Oguchi, I. Takeuchi, Y. Choi, J. S. Jiang, J. P. Liu, S. E. Lofland, D. Josell, and L. A. Bendersky, Phys. Rev. B **75**, 144429 (2007).
[13] S. H. Sun, C. B. Murray, D. Weller, L. Folks, and A. Moser, Science **287**, 1989 (2000).
[14] H. Zeng, J. Li, J. P. Liu, Z. L. Wang, and S. H. Sun, Nature (London) **420**, 395 (2002).
[15] M. Chen, J. P. Liu, and S. H. Sun, J. Am. Chem. Soc. **126**, 8394 (2004).
[16] C. B. Rong, D. Li, V. Nandwana, N. Poudyal, Y. Ding, Z. L. Wang, H. Zeng, and J. P. Liu, Adv. Mater. **18**, 2984 (2006).
[17] C. B. Rong, V. Nandwana, N. Poudyal, J. P. Liu, T. Saito, Y. Q. Wu and M. J. Kramer, J. Appl. Phys. **101**, 09K515 (2007).
[18] C. D. Dai, D. Eakins, N. Thadhani, and J. P. Liu, Appl. Phys. Lett. **90**, 071911 (2007).
[19] H. G. Rutz, F. G. Hanejko, and S. H. Luk, Met. Powder Rep. **49**, 40 (1994).
[20] G. E. Fougere, J. R. Weertman, and R. W. Siegel, Nanostruct. Mater. **5**, 127 (1995).
[21] G. F. Bocchini, Powder Metall. **42**, 171 (1999).
[22] K. Kondoh, T. Takikawa, and R. Watanabe, J. Jpn. Soc. Powder Powder Metall. **47**, 941 (2000).
[23] S. Kang, Z. Jia, and D. E. Nikles, Nano Lett. **2**, 1033 (2002).
[24] Q. Yan, T. Kim, A. Purkayastha, P. G. Ganesan, M. Shima, and G. Ramanath, Adv. Mater. **17**, 2233 (2005).
[25] S. B. Qadri, E. F. Skelton, A. W. Webb, N. Moulton, J. Z. Hu, and J. K. Furdyna, Phys. Rev. B **45**, 5670 (1992).
[26] S. H. Sun, H. Zeng, D. B. Robinson, S. Raoux, P. M. Rice, S. X. Wang, and G. X. Li, J. Am. Chem. Soc. **126**, 273 (2004).
[27] C. B. Rong, Y. Li, and J. P. Liu, J. Appl. Phys. **101**, 09K505 (2007).
[28] K. Elkins, D. Li, N. Poudyal, V. Nandwana, Z. Jin, K. Chen, and J. P. Liu, J. Phys. D **38**, 2306 (2005).
[29] H. M. Jaeger and S. R. Nagel, Science **255**, 1523 (1992).
[30] S. H. Whang, Q. Feng, and Y. Q. Gao, Acta Mater. **46**, 6485 (1998).
[31] J. Lyubina, I. Opahle, K. H. Muller, O. Gutfleisch, M. Richter, M. Wolf, and L. Schultz, J. Phys.: Condens. Matter **17**, 4157 (2005).
[32] C. B. Rong, V. Nandwana, N. Poudyal, Y. Li, J. P. Liu, Y. Ding, and Z. L. Wang, J. Phys. D **40**, 712 (2007).
[33] N. N. Greenwood and A. Earnshaw, *Chemistry of the Elements* (Butterworths/Heinemann, Oxford, 1997).
[34] B. E. Warren, *X-Ray Diffraction* (Dover, New York, 1990), Chap. 12.
[35] J. A. Christodoulides, P. Farber, M. Daniil, H. Okumura, G. C. Hadjipanayis, V. Skumryev, A. Simopoulos, and D. Weller, IEEE Trans. Magn. **37**, 1292 (2001).
[36] S. H. Whang, Q. Feng, and Y. Q. Gao, Acta Mater. **46**, 6485 (1998).
[37] Y. K. Takahashi, T. Ohkubo, M. Ohnuma, and K. Hono, J. Appl. Phys. **93**, 7166 (2003).
[38] Z. X. Tang, C. M. Sorensen, K. J. Klabunde, and G. C. Hadjipanayis, Phys. Rev. Lett. **67**, 3602 (1991).

[39] A. Z. Men'shikov, Y. A. Dorofeev, V. A. Kazantsev, and S. K. Sidorov, Fiz. Met. Metalloved. **38**, 505 (1974).

[40] T. Katayama, T. Sugimoto, Y. Suzuki, M. Hashimoto, P. de Haan, and J. C. Lodder, J. Magn. Magn. Mater. **104–107**, 1002 (1992).

[41] S. C. Chen, P. C. Kuo, S. T. Kuo, A. C. Sun, C. Y. Chou, and Y. H. Fang, IEEE Trans. Magn. **41**, 915 (2005).

[42] K. Williamson and W. H. Hall, Acta Metall. **1**, 22 (1953).

[43] K. O'Grady, M. El-Hilo, and R. W. Chantrell, IEEE Trans. Magn. **29**, 2608 (1993).

[44] A. Bollero, O. Gutfleisch, K.-H. Muller, L. Schultz, and G. Drazic, J. Appl. Phys. **91**, 8159 (2002).

[45] C. B. Rong, H. W. Zhang, B. G. Shen, and J. P. Liu, Appl. Phys. Lett. **88**, 042504 (2006).

[46] J. S. Jiang, J. E. Pearson, Z. Y. Liu, B. Kabius, S. Trasobares, D. J. Miller, S. D. Bader, D. R. Lee, D. Haskel, G. Srajer, and J. P. Liu, Appl. Phys. Lett. **85**, 5293 (2004).